Electronic Supporting Information
for

Cu_2O Facet Controlled Reactivity for Peroxidase-like Activity

Shivanand Chettri,[†a] Liang-Ting Wu,[†b] Sagarmani Rasaily,[a] Debesh Sharma,[a] Bikram Gurung,[a] Rajani Dewan,[c] Sudarsan Tamang,[a] Jyh-Chiang Jiang,[b] and Anand Pariyar[a]**

[a]*Department of Chemistry, Sikkim University, Tadong 737102, Gangtok, East Sikkim, India.*

[b]*Department of Chemical Engineering, National Taiwan University of Science and Technology, Taipei 106335, Taiwan.*

[c]*Department of Chemistry, St. Joseph's College, Darjeeling 734101, West Bengal, India.*

*E-mail: anandpariyar@gmail.com (AP); jcjiang@mail.ntust.edu.tw (JCJ)

Table of Contents

1. **General information:** All the chemicals purchased were of analytical grade and were used without further purification. $CuSO_4.5H_2O$, $Na_3(C_6H_5O_7).2H_2O$, $CuCl_2.2H_2O$, CH_3COOH, CH_3COONa and anhydrous dextrose were purchased from Thomas Baker, India. Anhydrous sodium carbonate, ethanol, acetonitrile, sodium dodecyl sulfate (SDS) and hydrogen peroxide (H_2O_2) were purchased from Merck, India. Polyvinylpyrrolidone (PVP) was purchased from Loba chemie, 3,3',5,5'-tetramethylbenzidine (TMB) and 2, 2'-azinobis (3 ethylbenzothiazoline-6-sulfonic acid) diammonium salt (ABTS) was purchased from Sigma Aldrich, India. Sodium hydroxide was purchased from SD Fine Chem. Limited and $NH_2OH.3HCl$ was purchased from Rankem chemicals. Acetate buffer used during the reaction was prepared in the laboratory.
2. **General Methods:** Powder X-ray diffraction (PXRD) analysis was performed in PANalytical high resolution X-ray diffractometer equipped with a Cu K_a radiation (λ = 1.5418 Å) at a scan rate of 5° min^{-1} operated at a voltage of 40 kV and current of 30 mA over the angle (2ϑ) ranging from 5° to 90°. Scanning electron microscopic (SEM) was performed using JSM-6360 Scanning Electron Microscope. X-ray Photoelectron Spectrometry (XPS) was performed on a Thermo Scientific - ESCALAB 250 xi Photoelectron Spectrometer. The binding energies of all peaks were corrected as compared with reference peak of graphitic C (1s) core level value of 284.5 eV. UV-Vis spectroscopy was carried out in PerkinElmer Lambda-25 spectrophotometer. FTIR was performed in Bruker Alpha FTIR spectrophotometer. The PL intensity measurement was carried out using LS55 PerkinElmer Fluorescence spectrophotometer.

3. Experimental Details:

The synthesis of five different morphologies of Cu_2O, *viz*., cubic (*c*-Cu_2O), octahedral (*o*-Cu_2O), rhombododecahedral (*r*-Cu_2O), cuboctahedral (*co*-Cu_2O) and spherical (*s*-Cu_2O) were done using previous reports in the literature with slight modifications.[1–4]

3.1. Synthesis of cubic Cu_2O (*c*-Cu_2O): In a typical synthesis, $CuSO_4.5H_2O$ (0.169 g, 0.68 mmol) was dissolved in 18 mL water followed by addition of PVP (0.400 g, 0.01 mmol) and the mixture was stirred for 20 min. To this, 1 mL mixture containing $Na_3(C_6H_5O_7).2H_2O$ (0.217 g, 0.70 mmol) and anhydrous Na_2CO_3 (0.127 g, 1.2 mmol) was added drop-wise to the previous solution. The colour of the resultant solution changed from pale to deep blue. After stirring for 15 min, the entire mixture was kept on a preheated water bath at 80 °C. Finally, 1 mL dextrose solution containing 0.252 g (1.4 mmol) of anhydrous dextrous was added drop-wise and stirred for 2 h. The brick red precipitate formed was washed several times with water and ethanol. The obtained product was dried in vacuum at 60 °C overnight. Yield = 0.037 g.

3.2. Synthesis of octahedral Cu_2O (*o*-Cu_2O): In a typical synthesis, $CuSO_4.5H_2O$ (0.169 g, 0.68 mmol) was dissolved in 18 mL water and PVP (3.60 g, 0.09 mmol) was added to it and stirred for 30 min. Then, 1 mL aqueous solution containing $Na_3(C_6H_5O_7).2H_2O$ (0.217 g, 0.70 mmol) and anhydrous Na_2CO_3 (0.127 g, 1.2 mmol) was added drop-wise to the previous solution which resulted in change in the colour of the mixture from pale to deep blue. After stirring for 15 min, the entire mixture was kept on a preheated water bath at 80 °C, to which 1 mL dextrose solution containing 0.252 g (1.4 mmol) of anhydrous dextrous was added drop-wise and stirred for 2 h. The brick red precipitate formed was washed extensively several times with water and ethanol to remove the capping agent. Finally, the obtained product was dried in vacuum at 60 °C overnight. Yield = 0.019 g.

3.3. Synthesis of spherical Cu_2O (*s*-Cu_2O): In a typical synthesis, $CuSO_4.5H_2O$ (0.169 g, 0.68 mmol) was dissolved in 18 mL water and PVP (7.20 g, 0.18 mmol) was added to it and stirred for 30 min. To this, 1mL mixture containing $Na_3(C_6H_5O_7).2H_2O$ (0.217 g, 0.70

mmol) and anhydrous Na_2CO_3 (0.127 g, 1.2 mmol) was added drop-wise to the previous solution. The colour of the resultant solution changed from pale to deep blue. After stirring for 15min, the entire mixture was kept on a preheated water bath at 80 °C. Finally, 1 mL dextrose solution containing 0.252 g (1.4 mmol) of anhydrous dextrous was added drop-wise and stirred for 2 h. The brick red precipitate formed was washed several times with water and ethanol. The obtained product was dried in vacuum at 60 °C overnight. Yield = 0.010 g.

3.4. Synthesis of rhombododecahedron Cu_2O (*r*-Cu_2O): In a typical synthesis, 0.5 mL aqueous solution of $CuCl_2.2H_2O$ (0.1 M) was added into a vial containing SDS (0.087 g, 0.3 mmol) in 6.92 mL of water. After complete dissolution of SDS, 0.18 mL NaOH (1 M) was added to the mixture which resulted in formation of light blue solution of $Cu(OH)_2$. Finally, 2.4 mL $NH_2OH.HCl$ (0.1 M) was quickly added and kept in a water bath set at 40 °C for 1 hr. The crude obtained was washed vigorously several times by a mixture of water and ethanol (1:1) at 5000 rpm. Yield = 0.014 g.

3.5. Synthesis of Cubo-octahedral Cu_2O (*co*-Cu_2O): In a typical synthesis, 0.2 mL $CuCl_2.2H_2O$ (0.1 M) and SDS (0.174 g, 0.6 mmol) was added into a vial containing 18.4 mL of deionised water and vigorously stirred until complete dissolution. Then, 0.5 mL of NaOH (1 M) was added which resulted in a light blue coloration of the solution, followed by addition of 0.9 mL of $NH_2OH.HCl$ (0.2 M). After aging the reaction for 2 h, the precipitate was washed by centrifugation several times using a mixture of water and ethanol (1:1) at 5000 rpm. Yield = 0.009 g.

4. Peroxidase Activity:

4.1. Using TMB as substrate: In a typical experiment, 150 µL of 1.0 mM TMB, 100 µL of the prepared Cu_2O (33 µg/mL), and 50 µL of 50.0 mM H_2O_2 were added into 2.7 mL of 0.2 M acetate buffer (pH 4.0) and the time-dependent absorbance was recorded for 30 min. The control experiments in absence of the catalyst and H_2O_2 were also carried out which gave negligible evolution of the peak at 652 nm for the oxidised substrate. A series of experiments were then carried out with different morphologies of Cu_2O. At least three sets for each were conducted to ensure homogeneity of each experiment.

4.2. Using ABTS as substrate: In a typical experiment, 150 µL of 1.0 mM ABTS, 100 µL of the prepared Cu_2O (33 µg/mL), and 50 µL of 50.0 mM H_2O_2 were added into 2.7 mL of 0.2 M acetate buffer (pH 4.0) and the time-dependent absorbance was recorded for 30 min. The control experiments in absence of the catalyst and H_2O_2 were also carried out which gave negligible evolution of the peak at 420 nm for the oxidised substrate.

5. Steady State Kinetic Study:

The steady-state kinetic assays were conducted at room temperature in a reaction solution with 33 µg/mL Cu_2O as catalyst in presence of H_2O_2 and TMB. The kinetic assays of different morphologies Cu_2O with TMB as the substrate were performed at a fixed concentration of 0.833 mM H_2O_2 and different concentrations of TMB (0.017, 0.033, 0.05, 0.067, 0.083, 0.1, 0.117 and 0.133 mM). Likewise, the kinetic assays of different morphologies of Cu_2O as catalyst with H_2O_2 as the substrate were performed at a fixed concentration of 0.05 mM TMB and different concentrations of H_2O_2 (0.833, 1.667, 2.5, 3.333, 4.167, 5, 5.833 and 6.667 mM).

6. SEM images and particle size distributions:

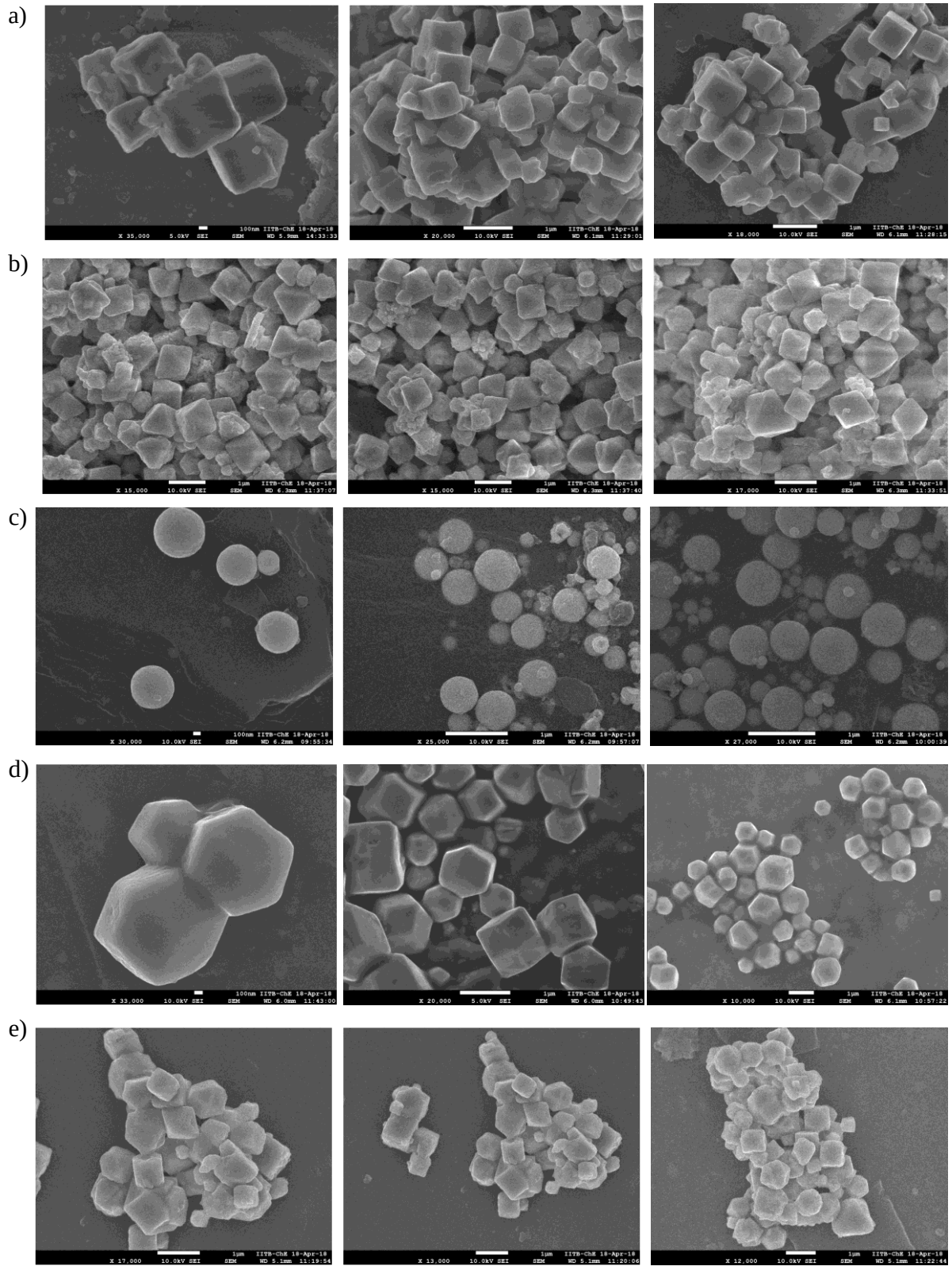

Fig. S1 SEM images of a) *c*-Cu_2O, b) *o*-Cu_2O, c) *s*-Cu_2O, d) *r*-Cu_2O and e) *co*-Cu_2O.

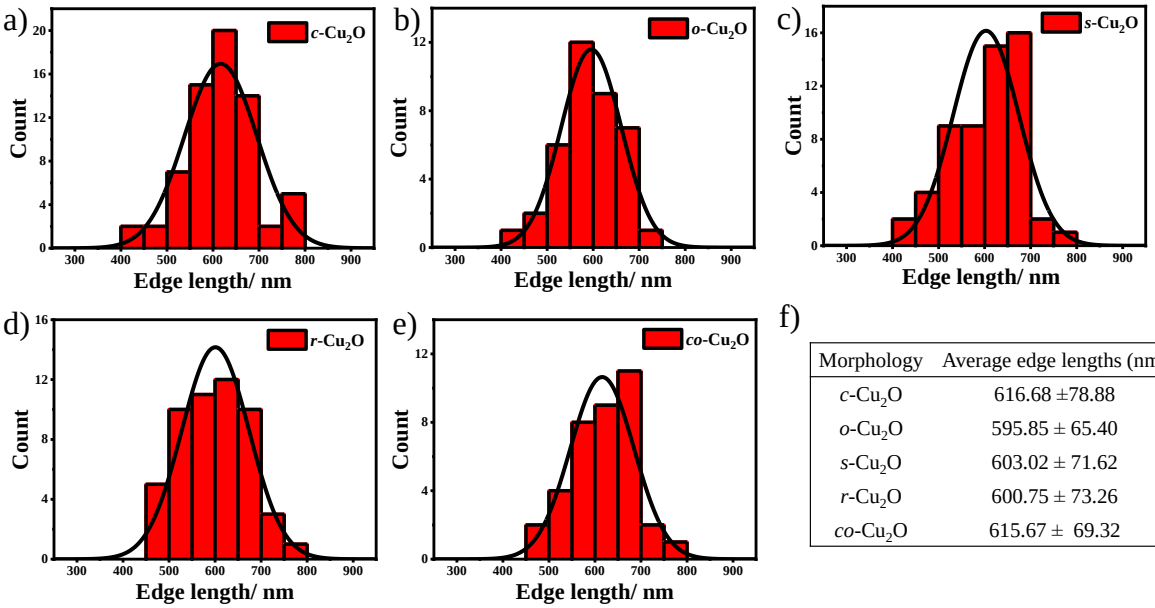

Morphology	Average edge lengths (nm)
c-Cu_2O	616.68 ±78.88
o-Cu_2O	595.85 ± 65.40
s-Cu_2O	603.02 ± 71.62
r-Cu_2O	600.75 ± 73.26
co-Cu_2O	615.67 ± 69.32

Fig. S2 Particle size distributions of a) *c*-Cu_2O, b) *o*-Cu_2O, c) *s*-Cu_2O, d) *r*-Cu_2O, e) *co*-Cu_2O and f) overview of average edge lengths of varied morphologies.

7. XPS of different Cu_2O

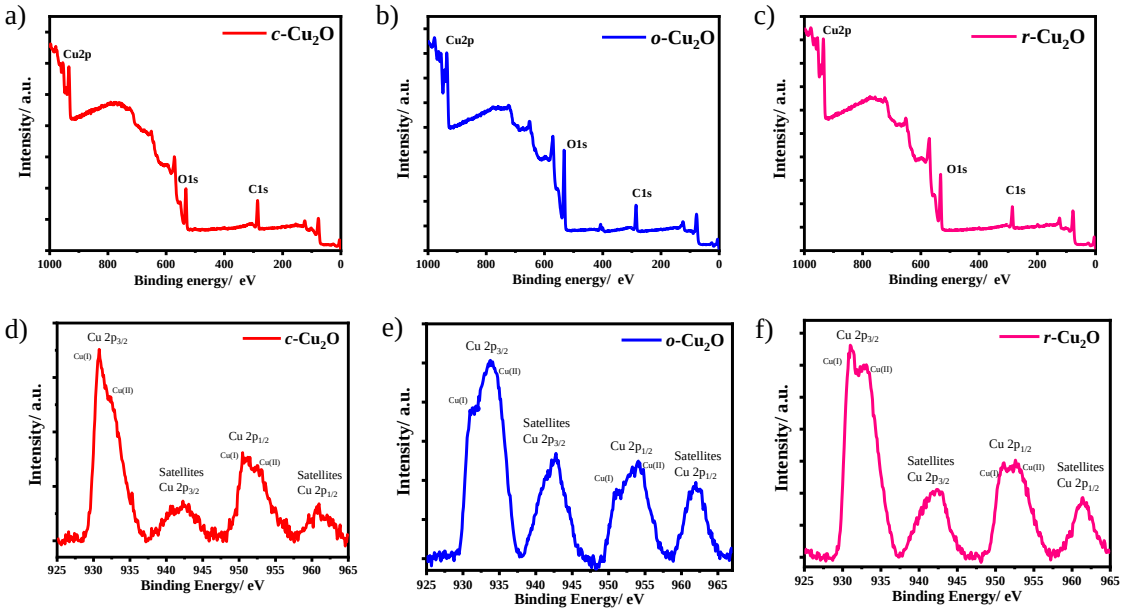

Fig. S3 XPS survey spectra of a) *c*-Cu_2O, b) *o*-Cu_2O and c) *r*-Cu_2O; The Cu 2p region of d) *c*-Cu_2O, e) *o*-Cu_2O and f) *r*-Cu_2O.

8. pH and temperature dependence on the peroxidase activity of Cu_2O:

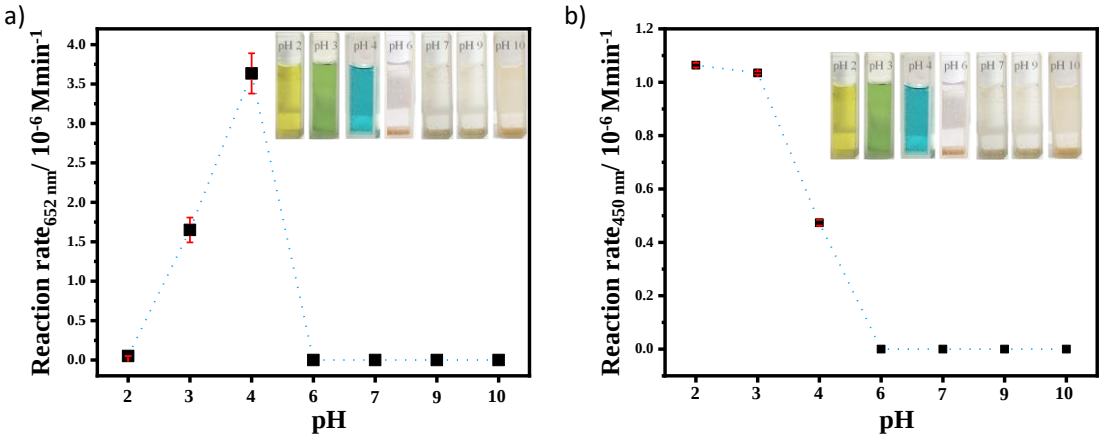

Fig. S4 pH dependence on the reaction rate of peroxidase activity as catalysed by *r*-Cu_2O for the formation of TMB_{ox} (λ_{max}= 652 nm) and $2e^-$ oxidised product ((λ_{max}= 450 nm).

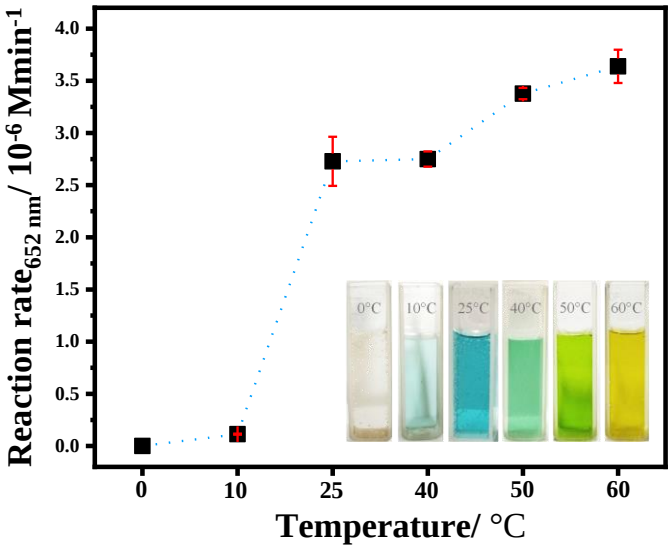

Fig. S5 Temperature dependence on the initial reaction rate of peroxidase activity as catalysed by *r*-Cu_2O for the formation of TMB_{ox} (λ_{max}= 652 nm).

9. Effect of catalytic loading on the peroxidase activity of Cu_2O:

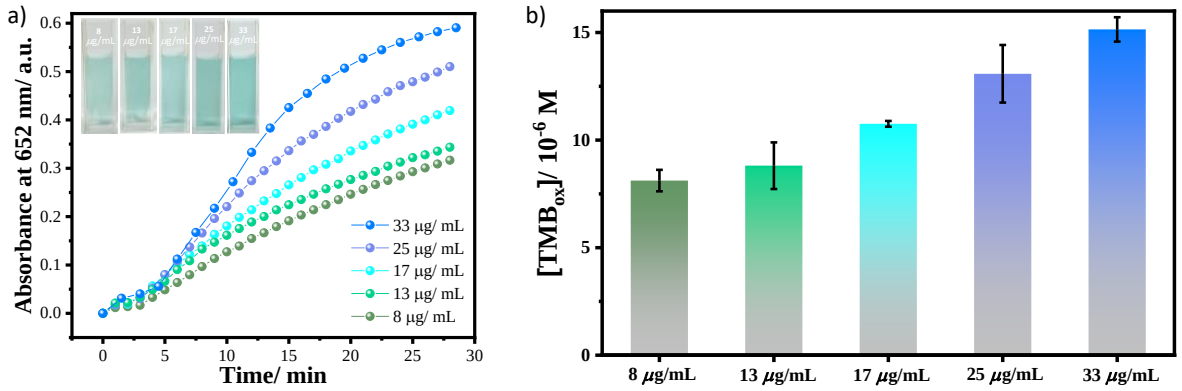

Fig. S6 Effect of catalytic loading on the peroxidase activity of *r*-Cu_2O in presence of H_2O_2 a) Time evolution of the absorbance of TMB_{ox} with respect to catalytic loading of 8-33 μg/mL of *r*-Cu_2O b) Concentration of TMB_{ox} measured at a time interval of 30 min. Here, the increase of induction time lowers turnover (within 30 min) for higher catalytic loading.

10. Peroxidase activity of different metal oxides:

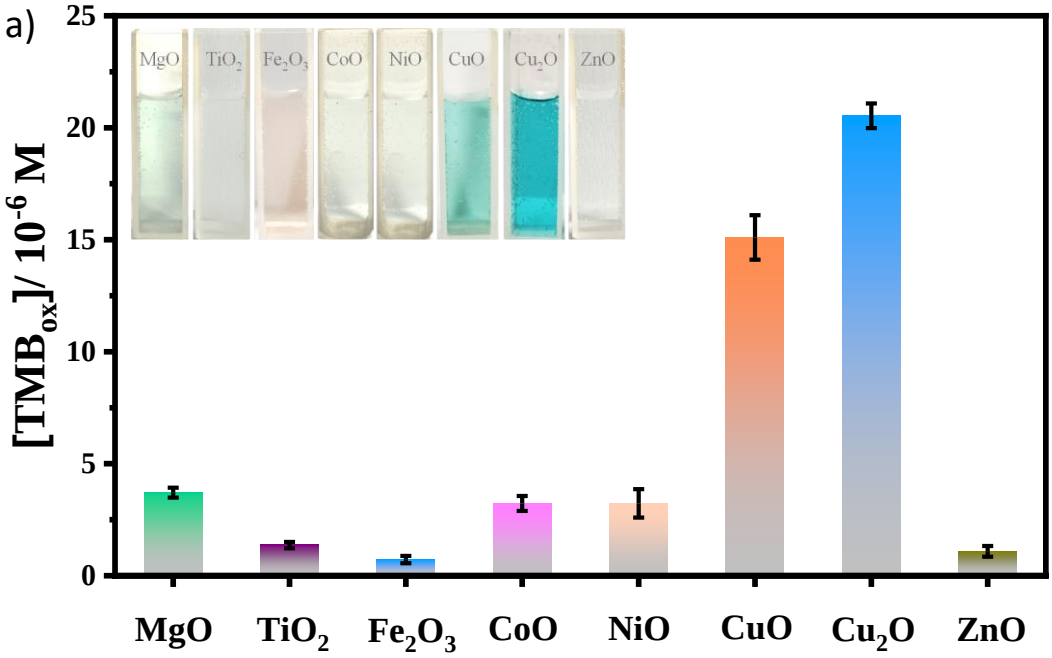

Fig. S7 Peroxidase activity of different metal oxides using 33 μg/mL catalytic loading, 0.05 mM TMB and 0.833 mM H_2O_2 in pH 4 acetate buffer at room temperature.

11. Comparison of reactivity of different Cu_2O under varied concentration of substrates.

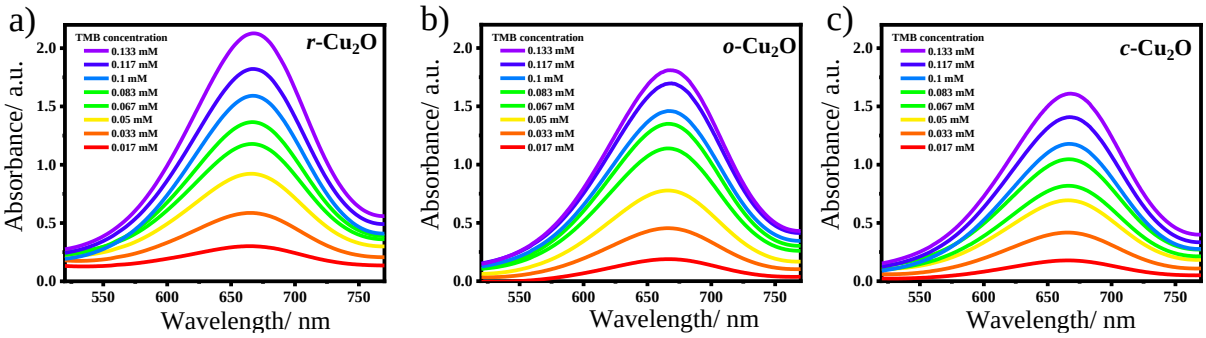

Fig. S8 Evolution of absorption band at t= 30 min for TMB_{ox} (λ_{max}= 652 nm) in presence of fixed H_2O_2 concentration of 0.83 mM and varied TMB concentration as catalysed by: a) *r*-Cu_2O, b) *o*-Cu_2O and c) *c*-Cu_2O.

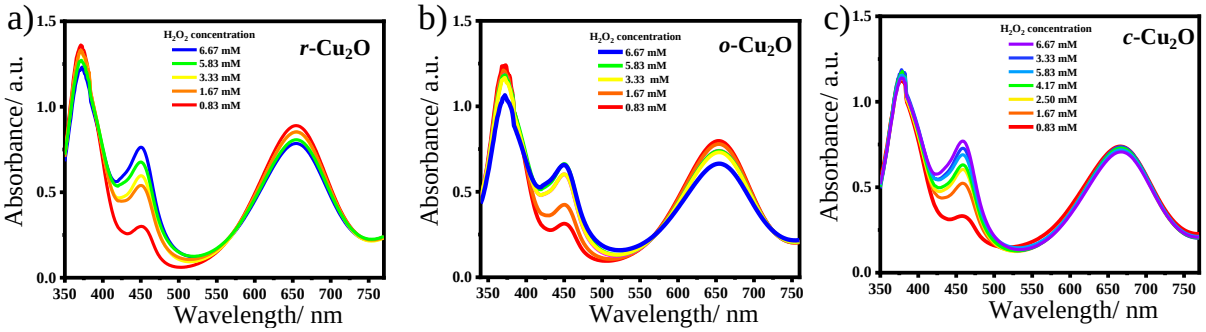

Fig. S9 Evolution of absorption band at t= 30 min for TMB_{ox} (λ_{max}= 652 nm) in presence of fixed TMB concentration of 0.05 mM and varied H_2O_2 concentration as catalysed by: a) *r*-Cu_2O, b) *o*-Cu_2O and c) *c*-Cu_2O.

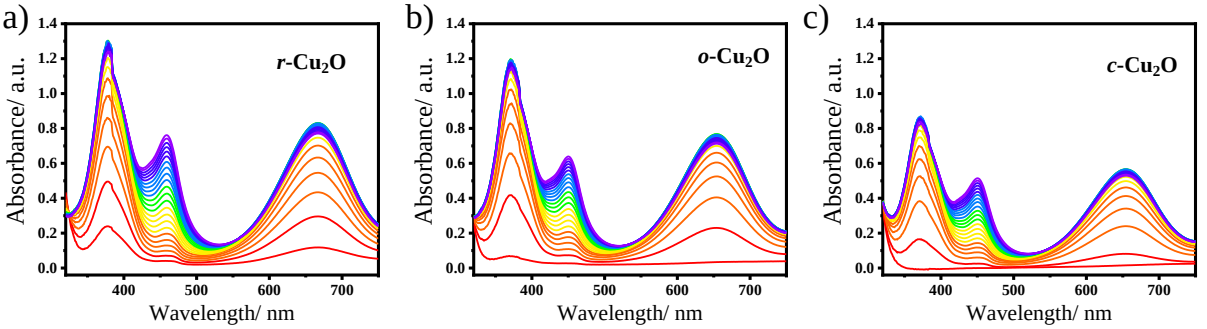

Fig. S10 Evolution of absorption band at t= 30 min for TMB_{ox} (λ_{max}= 652 nm) in presence of TMB concentration of 0.05 mM and H_2O_2 concentration of 4.17 mM as catalysed by: a) *r*-Cu_2O, b) *o*-Cu_2O and c) *c*-Cu_2O.

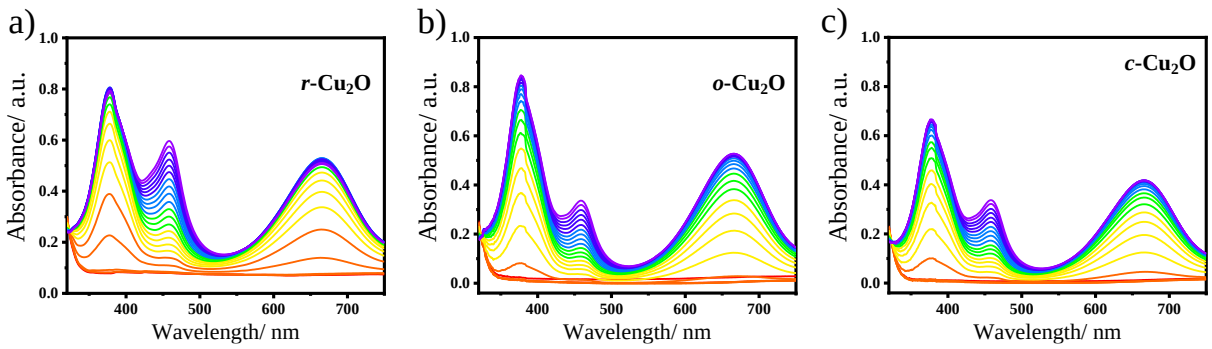

Fig. S11 Evolution of absorption band at t= 30 min for TMB_{ox} (λ_{max}= 652 nm) in presence of TMB concentration of 0.03 mM and H_2O_2 concentration of 1.67 mM as catalysed by: a) *r*-Cu_2O, b) *o*-Cu_2O and c) *c*-Cu_2O.

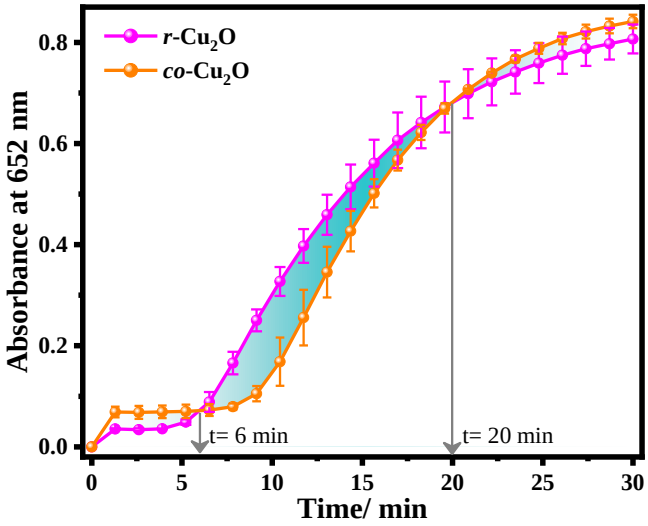

Fig. S12 Absorbance cross-over with *r*-Cu_2O and *co*-Cu_2O.

12. Detection of hydroxyl radical:

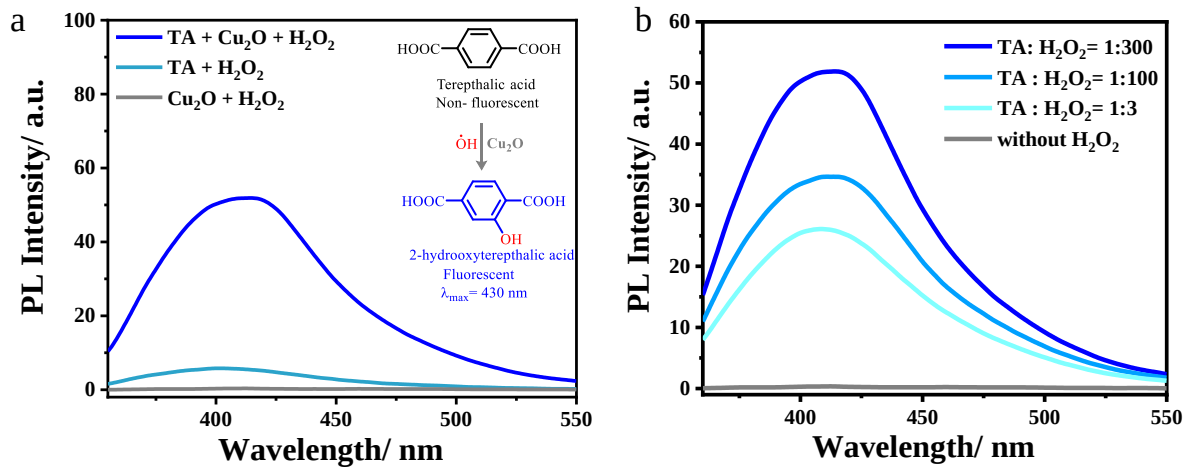

Fig. S13 a) PL intensity measured using terephthalic acid (TA) as a fluorescent probe for the generation of OH radicals (from added H_2O_2) in absence and presence of Cu_2O catalyst (Inset: Scheme for detection of hydroxyl radical by TA in presence of Cu_2O). b) Variation of PL intensity of 2-hydroxyterephthalic acid with respect to increasing concentration of H_2O_2 in presence of Cu_2O catalyst.

13. Computational Studies:

All spin-polarized density functional theory (DFT) calculations in this work were conducted using the Vienna ab initio Simulation Package (VASP)[5,6] with the projector augmented wave (PAW) method.[7,8] The exchange and correlation interactions were described using the generalized gradient approximation (GGA) functional of Perdew-Burke-Ernzerhof (PBE).[9] Additionally, Van der Waals corrections were applied using the DFT-D3 method.[10,11] A plane wave cutoff energy of 500 eV was employed, and Brillouin zone sampling was performed with the 3×3×1 Monkhorst-Pack grids for {100} and {111} facets, and 3×2×1 Monkhorst-Pack grids for the {110} facet.[12] The electronic energy convergence criterion was set to 10^{-4} eV for self-consistent iteration, and the force convergence criterion was set to 0.01 eV/Å for ionic relaxation. The transition states were located using the Climbing Image-Nudged Elastic Band (CI-NEB) method.[13,14] Frequency calculations were performed to verify stable structures and transition states, with a tighter energy convergence criterion of 10^{-5} eV used for SCF iteration during vibrational frequency calculation. In stable structures, all the vibration frequencies are positive, indicating a local minimum on the potential surface. For transition states, one imaginary frequency is required, corresponding to a first-order saddle point on the potential surface. To mimic real experimental conditions, we employed the implicit solvent model of water using VASPsol,[15,16] considering a dielectric constant of 78.4 when calculating the correction term associated with the implicit solvent. The total energy was corrected by accounting for zero-point energy and the implicit solvent effect using the following equation:

$$E = E_0 + k_B \sum_V \frac{\theta_V}{2} + \Delta E_{solv.}$$

where E represents the total energy, E_0 represents the electronic energy, ϑ_V represents the vibrational temperature of each vibrational mode, $\Delta E_{solv.}$ represents the electronic energy difference between the system in the gas phase and water solvent, and k_B represents the Boltzmann constant.

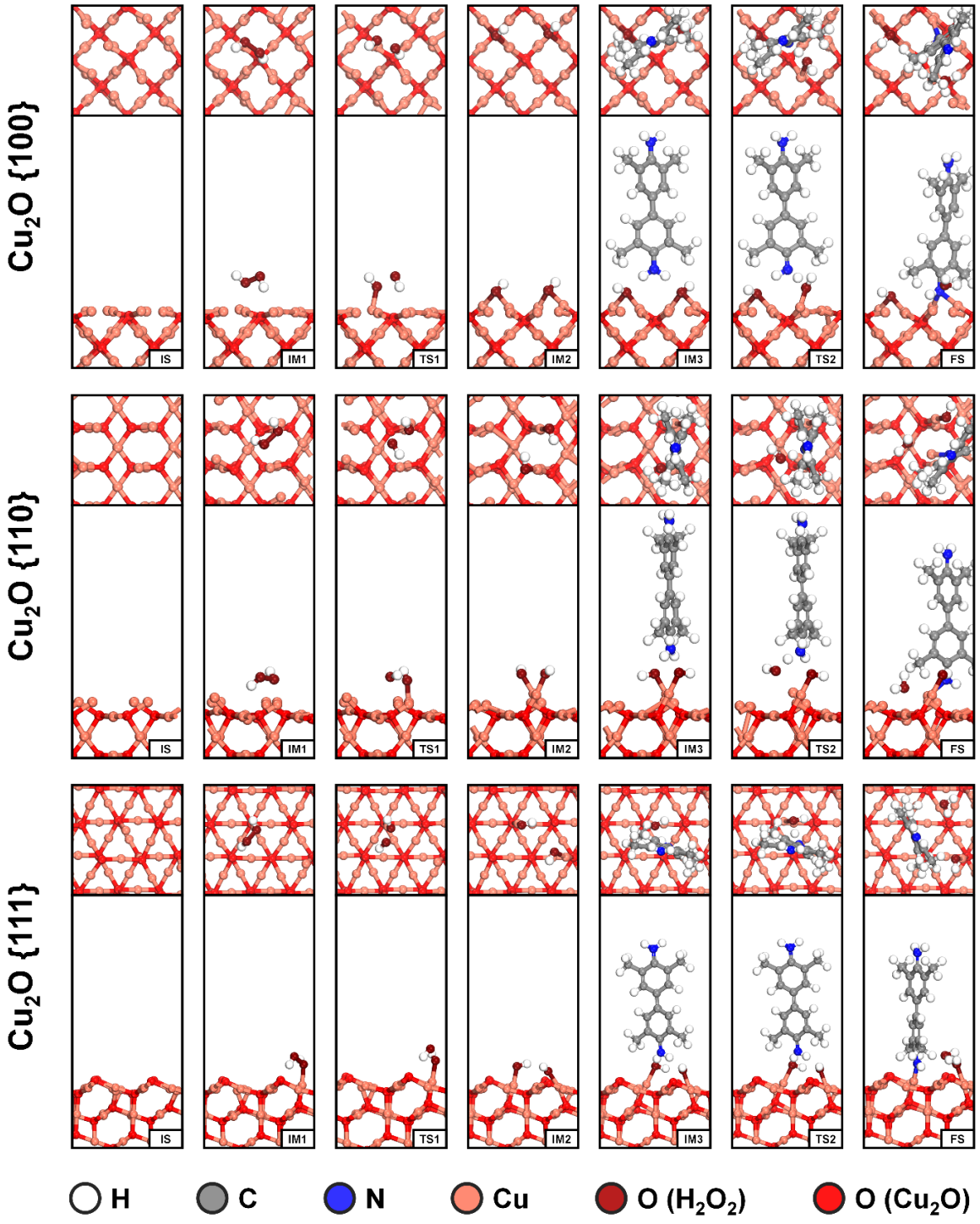

Fig. S14 Top and side views of optimized configurations of Cu_2O surfaces (IS), adsorbed intermediates (IM), transition states (TS), and the resulting products (FS) on three facets, {100}, {110}, and {111}. The white, gray, blue, orange, and red spheres represent the H, C, N, Cu, and O, respectively. The dark and bright red colors are used to distinguish O in H_2O_2 and Cu_2O.

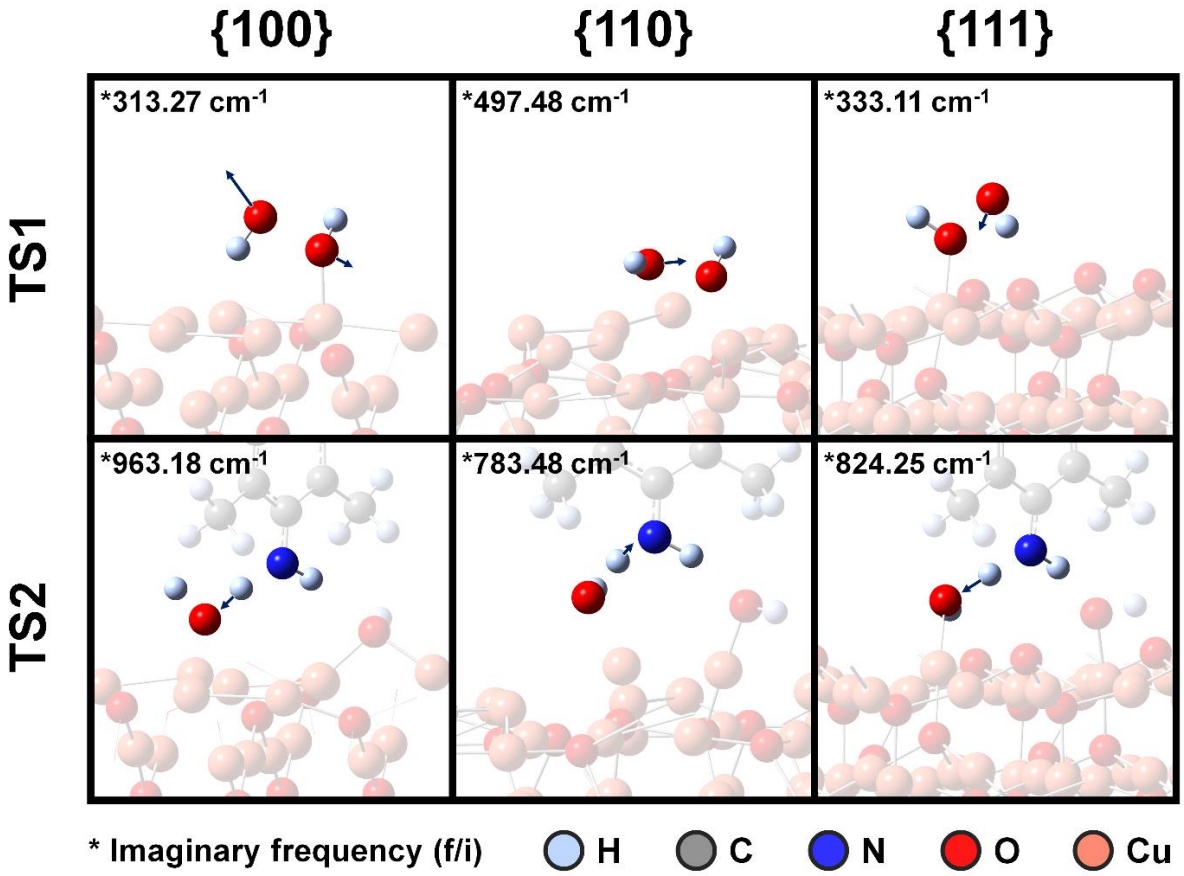

Fig. S15 The optimized configurations of TS1 and TS2 on Cu_2O {100}, {110}, and {111} exposed facets. The arrows in the figures represent the vibrational modes of the imaginary frequencies, corresponding to the reaction coordinates of the O-O cleavage and H radical transfer, respectively.

Table S1. The calculated total number of unsaturated atoms on the Cu_2O surface and the overall charge brought by unsaturated dangling Cu atoms.

Sl. No.	Facets	Surface Area (nm^2)	Total no. of unsaturated Cu atoms on the surface (coordination number, charge)	Total no. of unsaturated O atoms on the surface (coordination number)	Overall Charge on the surface brought by Cu
1	{110}	1.033	8 (1, 0.30 |e|)	0	2.37 |e|
2	{100}	0.731	8 (1, 0.26 |e|)	0	2.08 |e|
3	{111}	1.265	4 (1, 0.33 |e|)	4 (3)	1.31 |e|

Table S2. Calculated energetics of reaction coordinate for different facets of Cu_2O.

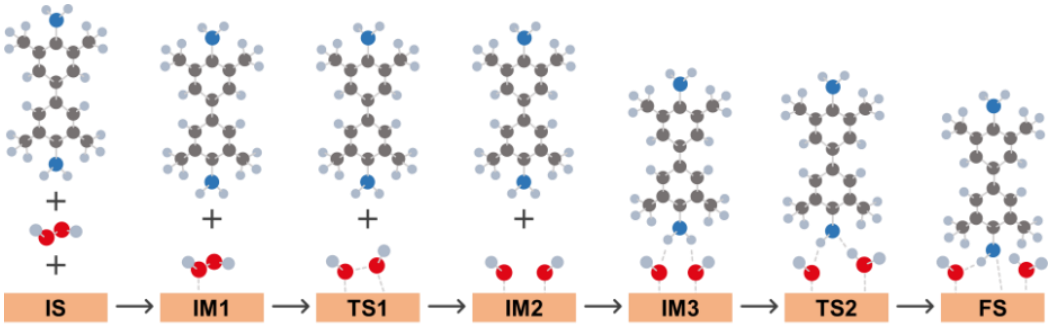

Facet	IS (eV)	IM1 (eV)	TS1 (eV)	IM2 (eV)	IM3 (eV)	TS2 (eV)	FS (eV)
{100}	0	-0.431	-0.371	-5.176	-5.840	-4.331	-6.184
{111}	0	-0.909	-0.656	-3.365	-4.137	-3.721	-4.365
{110}	0	-1.450	-1.296	-4.951	-5.683	-4.982	-5.358

14. References:

1 W. C. Huang, L. M. Lyu, Y. C. Yang and M. H. Huang, *J. Am. Chem. Soc.*, 2012, **134**, 1261–1267.

2 D. F. Zhang, H. Zhang, L. Guo, K. Zheng, X. D. Han and Z. Zhang, *J. Mater. Chem.*, 2009, **19**, 5220–5225.

3 Y. Sui, W. Fu, H. Yang, Y. Zeng, Y. Zhang, Q. Zhao, Y. Li, X. Zhou, Y. Leng, M. Li and G. Zou, *Cryst. Growth Des.*, 2010, **10**, 99–108.

4 C. H. Kuo and M. H. Huang, *J. Phys. Chem. C*, 2008, **112**, 18355–18360.

5 G. Kresse and J. Furthmüller, *Comput. Mater. Sci.*, 1996, **6**, 15–50.

6 G. Kresse and J. Furthmüller, *Phys. Rev. B - Condens. Matter Mater. Phys.*, 1996, **54**, 11169–11186.

7 P. E. Blöchl, *Phys. Rev. B*, 1994, **50**, 17953–17979.

8 D. Joubert, *Phys. Rev. B - Condens. Matter Mater. Phys.*, 1999, **59**, 1758–1775.

9 J. P. Perdew, K. Burke and M. Ernzerhof, *Phys. Rev. Lett.*, 1996, **77**, 3865–3868.

10 S. Grimme, J. Antony, S. Ehrlich and H. Krieg, *J. Chem. Phys.*, 2010, **132**, 154104–154119.

11 S. GRIMME, S. EHRLICH and L. GOERIGK, *J. Comput. Chem.*, 2012, **32**, 174–182.

12 J. D. Pack and H. J. Monkhorst, *Phys. Rev. B*, 1977, **16**, 1748–1749.

13 G. Henkelman, B. P. Uberuaga and H. Jónsson, *J. Chem. Phys.*, 2000, **113**, 9901–9904.

14 G. Henkelman and H. Jónsson, *J. Chem. Phys.*, 2000, **113**, 9978–9985.

15 K. Mathew, R. Sundararaman, K. Letchworth-Weaver, T. A. Arias and R. G. Hennig, *J. Chem. Phys.*, 2014, **140**, 0–8.

16 K. Mathew, V. S. C. Kolluru, S. Mula, S. N. Steinmann and R. G. Hennig, *J. Chem. Phys.*, 2019, **151**, 234101–234108.